

Determination of the static polarizability of the $8s^2S_{1/2}$ state of atomic cesium

Mevan Gunawardena

School of Electrical and Computer Engineering, Purdue University, West Lafayette, Indiana 47907, USA

D. S. Elliott

*School of Electrical and Computer Engineering, Purdue University, West Lafayette, Indiana 47907, USA;
Department of Physics, Purdue University, West Lafayette, Indiana 47907, USA*

M. S. Safronova

Department of Physics and Astronomy, University of Delaware, Newark, Delaware 19716, USA

U. Safronova

Department of Physics, University of Nevada, Reno, Nevada 89557, USA

(Received 15 August 2006; revised manuscript received 5 December 2006; published 20 February 2007)

We report a precise determination of the static polarizability of the $8s^2S_{1/2}$ state of atomic cesium, carried out jointly through experimental measurements of the dc Stark shift of the $6s^2S_{1/2} \rightarrow 8s^2S_{1/2}$ transition using Doppler-free two-photon absorption and theoretical computations based on a relativistic all-order method. We enhance the precision of the measurement by imposing phase-modulation sidebands on the laser beam and by using a pair of vapor cells, one of which serves as a reference, and measuring the absorption spectrum in each cell with a single scan of the laser frequency. The measured value for the polarizability of the $8s$ state is $38,060 \pm 250 a_0^3$, in very good agreement with our theoretical value of $38,260 \pm 290 a_0^3$. In addition, the small difference in the Stark shift measurement for the two hyperfine states that we examine yields a variation in the polarizability due to the magnetic dipole contact interaction of $290 \pm 30 a_0^3$.

DOI: [10.1103/PhysRevA.75.022507](https://doi.org/10.1103/PhysRevA.75.022507)

PACS number(s): 32.10.Dk, 32.60.+i, 32.10.Fn

I. INTRODUCTION

Atomic cesium has played a central role in a wide variety of precision measurements, including those of parity nonconserving interactions (PNC) [1–3], the search for a permanent electric dipole moment [4], and transition frequencies for use in atomic clocks [5,6]. Much effort has already been put into obtaining accurate values of transition dipole moments [7] and polarizabilities [8,9] for the $6s^2S_{1/2} \rightarrow 7s^2S_{1/2}$ transition, which has been the cornerstone for many of the parity violation experiments. The ground-state polarizability of $401.0 a_0^3$ is now known to a precision of 0.15% [10], whereas that of the $7s$ state ($5837 \pm 7 a_0^3$) is an 0.12% determination [8]. Both these values are in very good agreement with theory [11–13]. Recent measurements and calculations of the transition moments of the $6p^2P_j \rightarrow 8s^2S_{1/2}$ transitions are in good agreement with one another [14]. Van Wijngaarden and Li [15] report measurements and calculations of the polarizabilities of excited $ns^2S_{1/2}$ states for $n=10-13$. They cite an experimental uncertainty of typically 0.1%, but calculated results are typically within 1% agreement with experiment.

The potential energy of an atom or nondipolar molecule in a static electric field of magnitude E_0 is decreased by an amount

$$\Delta W = -\frac{1}{2} \alpha E_0^2, \quad (1)$$

where α is the polarizability of the atom. In this work, we investigate the polarizability of the $8s^2S_{1/2}$ state in cesium and report an experimental value of $38,060 \pm 250 a_0^3$, representing a precision of 0.7%. This is in excellent agreement with results of our theoretical calculations, $38,260 \pm 290 a_0^3$.

We carry out our laboratory determination through measurements of the dc quadratic Stark shift of the $6s^2S_{1/2} \rightarrow 8s^2S_{1/2}$ transition using a Doppler-free two-photon technique. We achieve improved resolution in the determination of the frequency shifts in this technique by phase modulating the laser beam that drives the interaction and using, in addition to the Stark cell, a second reference cell, reducing any errors due to laser frequency drifts and scan nonlinearities.

We discuss the experimental measurement of the polarizability in Sec. II, and the theoretical determination of this quantity in Sec. III. In Sec. IV, we discuss the small difference we observe between the polarizability of the $F=3$ and $F=4$ components.

II. EXPERIMENT

We show the experimental setup in Fig. 1. A scannable, frequency-stabilized, ring cw Ti:Sapphire laser produces a beam at 822.46 nm with a power of ~ 135 mW, which we focus first into a Stark cell (a glass cesium vapor cell fitted with internal parallel plate electrodes) and again into a reference cesium cell. The beam is reversed back on itself after exiting the reference cell. An optical isolator placed at the exit of the laser prevents the retroreflected beam from coupling back into the laser. The beam profile is Gaussian in shape, with a beam radius (corresponding to an intensity e^{-2} of the on-axis intensity) of $175 \mu\text{m}$ in the Stark cell and $120 \mu\text{m}$ in the reference cell. We maintain the temperature of the cold finger on the Stark cell at 38°C , while that of the reference cell is around 50°C , corresponding to atomic den-

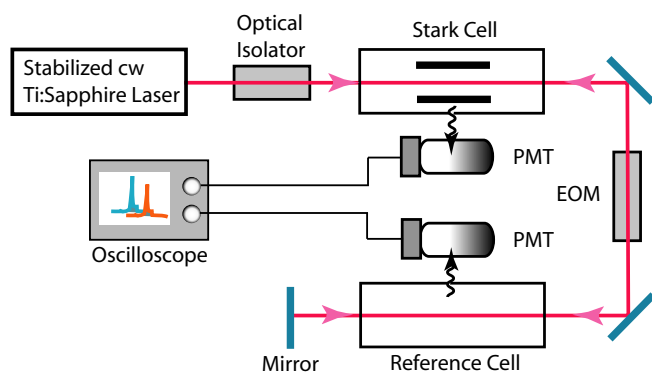


FIG. 1. (Color online) The experimental setup. The output of the cw stabilized Ti:Sapphire laser passes through the Stark cell and the reference cell in both directions for a Doppler-free two-photon absorption measurement. Phase modulation in the electro-optic modulator (EOM) imposes rf sidebands on the laser. The fluorescence emission upon spontaneous decay of the $8s$ state is detected with the photomultipliers (PMT).

sities of $1.4 \times 10^{11} \text{ cm}^{-3}$ and $4 \times 10^{11} \text{ cm}^{-3}$, respectively. From each of these cells, we collect the fluorescent radiation at 794.6 nm ($8s^2S_{1/2} \rightarrow 6p^2P_{3/2}$ transition) from the side using a pair of plano convex lenses, an interference filter, a spatial aperture, and a photomultiplier tube (PMT). The length of the interaction region imaged onto the spatial aperture is ~ 8 mm. The branching ratio for decay of the $8s^2S_{1/2}$ state by this fluorescence pathway is 41.3% [16]. We observe and record the output of the photomultiplier tubes using a digitizing oscilloscope (input impedance = 1 M Ω) vs frequency of the tunable laser. We estimate the overall collection efficiency of our detection system, including the solid angle factor, transmission of our optics and aperture, and the quantum efficiency of the PMT, to be $\sim 0.1\%$. Detected noise consists primarily of dark current from the PMT (~ 25 mV) and scattered laser light that reaches the PMT (~ 175 mV). We measure magnetic fields in the region of the vapor cell to be < 1 G.

The Stark cell is constructed of Pyrex, with the stainless-steel field plates of dimension 2.54 cm by 1.52 cm mounted on tungsten electrical feedthroughs fused to the body of the cell. The spacing between the plates is nominally 5 mm ($0.201'' \pm 0.0005''$ at one end and $0.187'' \pm 0.0005''$ at the other). The cell was designed for another purpose that did not require highly parallel surfaces, and in retrospect, the precision in our measurements of the Stark shift would have been much greater had the field plates been more parallel to one another. We shall return to this point later in this report. We measure the voltage between the plates using an $\sim 1:1000$ high-voltage dividing probe. Using an Agilent 34410A multimeter with a specified accuracy of better than 0.03%, we checked the calibration of this probe and found it to be 1:1004.

Before each measurement, we establish the scan linearity and precise calibration of the laser frequency ν_L as a function of time by phase modulating the laser at modulation frequency ν_m , imposing sidebands on the laser spectrum at $\nu_L \pm n\nu_m$, for $n=0, 1, 2, \dots$, etc., which become our frequency reference markers. We vary the modulation fre-

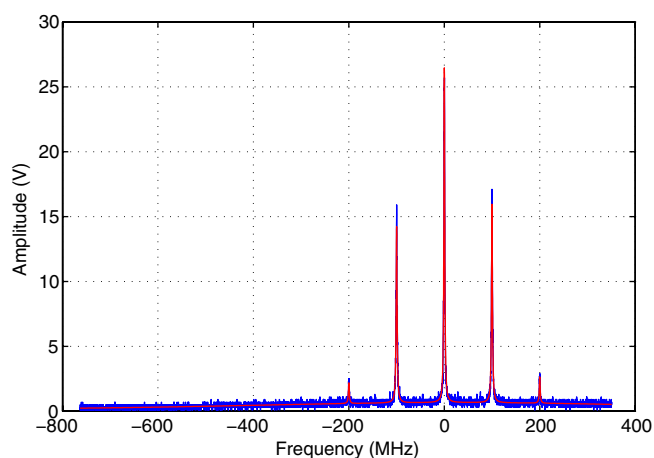


FIG. 2. (Color online) Typical two-photon absorption spectrum of atomic cesium in the reference cell resulting from a phase-modulated laser. The modulation frequency for this example is 100 MHz, resulting in sidebands at spacings of 100 MHz.

quency in 10 MHz steps from 10 MHz to 300 MHz and show a typical two-photon absorption spectrum recorded with this phase-modulated laser field in Fig. 2. The frequency spacing between peaks in this spectrum, when plotted as a function of atomic frequency (twice the laser frequency, since we excite this transition through a two-photon absorption interaction), is ν_m . When fitted to a computed spectrum consisting of five narrow Lorentzian line shapes and a low-level Doppler-broadened background (resulting when atoms absorb both photons from just one laser beam), we are able to calibrate the laser frequency to within an uncertainty of 0.4 MHz. In order to account for a slight non-linearity of the laser scan, we use a fourth-order polynomial to calibrate the frequency. Several different polynomial models were tested, and the fourth-order polynomial gave the minimum uncertainty in the determination of the frequency.

To carry out the measurements of the Stark shift, we apply a voltage of 0 to 5 kV in steps of 0.25 kV across the electrodes of the Stark cell and scan the laser frequency through the cesium two-photon resonance for both the Stark and the reference cells. We carry out the measurements of the dc Stark shift separately for the $F=3 \rightarrow F'=3$ and the $F=4 \rightarrow F'=4$ transitions using linearly polarized light, with separate calibration of the frequency scan as described in the previous paragraph in these two spectral regions. We show a series of these Stark-shifted resonances in Fig. 3. The scan width is 560 MHz at 2 s per scan, consisting of 10 000 data points. We choose this slow scan speed in order to minimize distortions to the absorption line shapes that might arise from the time constant of our detection system (30 μs). We obtain the peak frequency for the Stark-shifted resonance by fitting a narrow Lorentzian line shape and a Doppler broadened background profile to the measured spectrum. At low applied voltages, the linewidth of the two-photon absorption line is ~ 2.1 MHz, within 10% of the 1.83 MHz lifetime-limited linewidth expected for the measured lifetime of 87 ns for the $8s^2S_{1/2}$ state [17]. As we increase the voltage on the Stark cell, the absorption profile shows a broadening and a slight asymmetry due to the nonparallel plate separation, giving

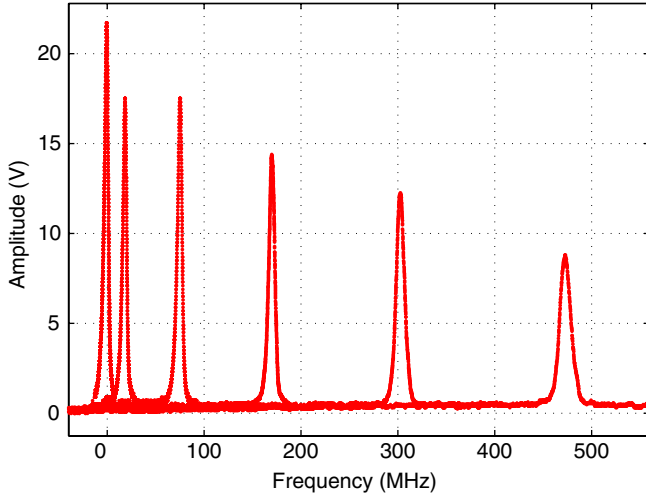


FIG. 3. (Color online) Scans of the Stark-shifted two-photon absorption spectrum cell at 0–5 kV, in steps of 1 kV.

rise to a linearly varying electric field in the fluorescence collection region. Tracing the optical pathway of the fluorescence radiation from the interaction region to the detector allows us to determine the relative collection efficiency from different regions within the interaction region, and we are able to reproduce the line shapes with good reliability. The difference in the peak positions of the two-photon spectrum in the Stark cell and that in the reference cell is a measure of the Stark shift. The maximum linewidth, which we observed at the largest applied field, was ~ 10 MHz.

We show in Fig. 4 a plot of the measured Stark shift versus the square of the dc electric field for the $F=4 \rightarrow F'=4$ transition. A linear fit to these data yields a Stark shift of 4.701 ± 0.003 MHz(kV/cm) $^{-2}$ (in atomic frequency units), where the uncertainty reflects the statistical distribution of the data, but does not include the uncertainty due to imprecision in the determination of the spacing of the parallel plates. The dotted-dashed curve shows the deviation between the experimental data and a straight-line fit. Analysis

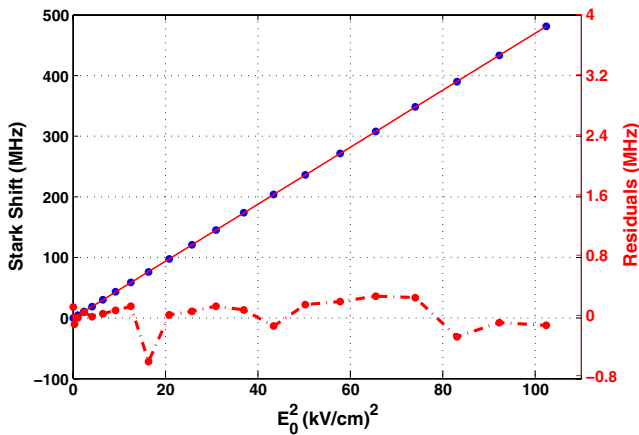


FIG. 4. (Color online) Stark shift versus the square of the dc electric field applied to the cell, for the $F=4 \rightarrow F'=4$ transition. The dotted-dashed curve shows the deviation between the experimental data and a straight line fit.

of the Stark shift of the $F=3 \rightarrow F'=3$ transition yields a similar result, with a measured Stark shift of 4.665 ± 0.003 MHz(kV/cm) $^{-2}$. Using the weighted average of these two values, as well as the ground-state polarizability of $401a_0^3 = 0.0998$ MHz(kV/cm) $^{-2}$ [10], we determine the average polarizability of the $8s^2S_{1/2}$ state to be $\alpha_0 = 9.470 \pm 0.060$ MHz(kV/cm) $^{-2}$, or $38\,060 \pm 250a_0^3$. The 0.7% uncertainty in our measurement of α_0 is primarily due to the spacing of the parallel plates in our vapor cell. Other factors contributing to the experimental uncertainty in α_0 include the determination of the peak of the two-photon absorption spectral resonances, 0.2% average; frequency calibration of the laser scan, 0.15%; calibration of the voltmeter, 0.06%; attenuation factor of the voltage probe, 0.01%.

III. THEORY

The scalar polarizability α_0 of the Cs atom in the $8s$ state can be calculated as the sum of the polarizability of the ionic core α_0^c and the valence polarizability α_0^v

$$\alpha_0 = \alpha_0^c + \alpha_0^v.$$

The core contribution was calculated in the random-phase approximation (RPA) in [18] and is very small, $16a_0^3$. A counterterm compensating for excitations from the core to the valence shell that violate the Pauli principle is negligible for the $8s$ state and can be omitted without loss of accuracy. The valence contribution to the polarizability is calculated in a sum-over-state approach as

$$\alpha_0^v = \frac{1}{3} \sum_n \frac{\langle n || D || 8s \rangle^2}{E_n - E_{8s}}, \quad (2)$$

where D is the dipole operator. The sum over the intermediate states n in Eq. (2) converges very rapidly, and only the first several terms are important. Therefore, the calculation of the $8s$ static polarizability reduces to the calculation of the $\langle np_j || D || 8s \rangle$ reduced electric-dipole matrix elements.

We conduct the calculation of the required matrix elements using the relativistic all-order method that includes single and double (SD) excitations of Dirac-Fock (DF) wave functions to all orders in perturbation theory. The dominant corrections not included within the framework of the SD all-order method are evaluated for dominant transitions. We refer the reader to Refs. [9,19,20] for a detailed description of the all-order method and its extensions. Briefly, the wave function of the valence electron v is represented as an expansion

$$|\Psi_v\rangle = \left[1 + \sum_{ma} \rho_{ma} a_m^\dagger a_a + \frac{1}{2} \sum_{mnab} \rho_{mnab} a_m^\dagger a_n^\dagger a_b a_a + \sum_{m \neq v} \rho_{mv} a_m^\dagger a_v + \sum_{mma} \rho_{m m v a} a_m^\dagger a_n^\dagger a_a a_v \right] |\Phi_v\rangle, \quad (3)$$

where Φ_v is the lowest-order (DF) atomic wave function. The indices m and n designate excited states and indices a and b designate core states. The equations for the excitation coefficients ρ_{ma} , ρ_{mv} , ρ_{mnab} , and $\rho_{m m v a}$ are solved iteratively until the correlation energy converges to the required accu-

TABLE I. The absolute values of the $8s-7p_j$ and $8s-8p_j$ electric-dipole matrix elements calculated in various approximations. The lowest-order matrix elements are listed in the column labeled “DF.” The *ab initio* all-order values calculated in single-double (SD) approximation and with partial inclusion of the triple excitations (SDpT) are given. The corresponding scaled values are listed in column labeled “SD scaled” and “SDpT scaled.” All values are given in atomic units (a_0e , where a_0 is the Bohr radius).

Transition	DF	SD	SDpT	SD _{sc}	SDpT _{sc}
$8s-7p_{1/2}$	9.534	9.251	9.290	9.313	9.291
$8s-7p_{3/2}$	14.281	13.996	14.035	14.066	14.039
$8s-8p_{1/2}$	18.634	17.710	17.841	17.777	17.752
$8s-8p_{3/2}$	25.857	24.460	24.659	24.564	24.528

racy. The electric-dipole matrix elements are expressed as the linear or quadratic functions of the excitation coefficients. The triple excitation term

$$\frac{1}{6} \sum_{mnrab} \rho_{mnrab} a_m^\dagger a_n^\dagger a_r^\dagger a_b a_a a_v |\Phi_v\rangle \quad (4)$$

is partially included into the values that we label “SDpT” in the text and Table I.

We find that the $8s-7p_j$ and $8s-8p_j$ transitions overwhelmingly give the dominant contributions to the $8s$ scalar polarizability. Therefore, we study these transitions in more detail. We find that for all of these transitions, a single correlation correction term containing only single excitation coefficients ρ_{mv} is dominant. The SDpT method in its current implementation is aimed precisely at correcting this contribution. Therefore, we have conducted the SDpT calculation for these terms. For the other transitions, $8s-6p$, $8s-9p$, $8s-10p$, $8s-11p$, and $8s-12p$, our SD results are sufficiently accurate and no further calculations were necessary. We also conducted a semiempirical scaling procedure for both SD and SDpT results that is aimed at estimating the dominant missing contributions. In this procedure, the single excitation coefficients ρ_{mv} are rescaled with the ratios of the all-order “experimental” to theoretical correlation energies for the specific state v and the calculation of the electric-dipole matrix elements is repeated with the modified coefficients. The experimental correlation energy is defined as a difference between the experimental energy and the DF value. The scaling procedure is described, for example, in Ref. [9], and references therein.

The results for the dominant transitions are summarized in Table I. The lowest-order matrix elements are listed in the column labeled “DF.” The *ab initio* all-order values calculated in single-double (SD) approximation and with partial inclusion of the triple excitations (SDpT) are given together with the corresponding scaled values. We take SD_{sc} values as our final results based on the extensive comparison of similar transition matrix elements for other monovalent systems with various types of experiments [9,14,21,22]. The uncertainty of each matrix element is estimated as the maximum difference between the final values and the SD, SDpT, and SDpT_{sc} data.

TABLE II. Contributions to the $8s$ scalar polarizability α_0 in Cs and their uncertainties $\delta\alpha_0$ in a_0^3 . The absolute values of the corresponding electric-dipole reduced matrix elements are also given.

Contribution	$\langle n D 8s\rangle$	α_0	$\delta\alpha_0$
$6p_{1/2}$	1.026	-6	0
$6p_{3/2}$	1.461	-12	0
$7p_{1/2}$	9.313	-2487	33
$7p_{3/2}$	14.066	-6106	60
$8p_{1/2}$	17.777	16609	125
$8p_{3/2}$	24.564	29935	253
$9p_{1/2}$	1.741	67	3
$9p_{3/2}$	2.970	192	8
$10p_{1/2}$	0.672	8	1
$10p_{3/2}$	1.240	25	3
$11p_{1/2}$	0.375	2	0
$11p_{3/2}$	0.726	8	1
$12p_{1/2}$	0.248	1	0
$12p_{3/2}$	0.495	3	0
Core		16	2
Tail		9	9
Final		38260	290

Contributions to the $8s$ scalar polarizability α_0 in Cs and their uncertainties $\delta\alpha_0$ are given in Table II. The absolute values of the corresponding electric-dipole reduced matrix elements are also given. We use the energies from [23] for all contributions with $n < 13$. The relative uncertainty of each polarizability term is twice the relative uncertainty of the corresponding matrix element. The uncertainties of the four main contributions are determined as described above. The uncertainties for all other terms are very small and are determined based on the size of the correlation correction for the particular transition. The contributions of terms with $n > 12$ are negligible; they are calculated in the DF approximation and are listed together in the row labeled “Tail.” Our final theoretical value $\alpha_0 = 38\,260 \pm 290 a_0^3$ is an excellent agreement with the experimental value $\alpha_0 = 38\,060 \pm 250 a_0^3$.

IV. HYPERFINE EFFECTS

The difference between the Stark shift of the $F=3 \rightarrow F'=3$ and the $F=4 \rightarrow F'=4$ transitions that we measure, while small (they differ by only 0.8%), is yet statistically significant. Sandars [24] considered the effect of the hyperfine interaction on the polarizability in 1967. For an alkali metal atom in an s -state (with nuclear angular momentum I , electronic angular momentum, $J = \frac{1}{2}$, and total angular momentum $F = I + \frac{1}{2}$), α can be expressed in the form

$$\alpha(F = I + \frac{1}{2}, m_F) = \alpha_0 + \alpha_{10} + \frac{3m_F^2 - (I + \frac{1}{2})(I + \frac{3}{2})}{I(2I + 1)} (\alpha_{12} + \alpha_{02}), \quad (5)$$

while for an s -state of total angular momentum $F = I - \frac{1}{2}$, it can be written as

$$\begin{aligned} \alpha(F=I-\frac{1}{2}, m_F) &= \alpha_0 - \frac{I+1}{I} \alpha_{10} + \frac{3m_F^2 - (I^2 - \frac{1}{4})}{(I-1)(2I-1)} \\ &\times \left\{ \frac{(2I-1)(I-1)}{I(2I+1)} \alpha_{12} + \frac{(2I+3)(I-1)}{I(2I+1)} \alpha_{02} \right\}. \quad (6) \end{aligned}$$

The different terms for the polarizability come from the division of the electronic part of the hyperfine operator into spin and orbital parts and then classifying terms by the ranks of the corresponding tensors. α_0 is the average polarizability, as one would find in the absence of hyperfine effects, and was the subject of Secs. II and III of this paper. α_{10} is the contribution to α due to a magnetic dipole contact potential and leads to a slight difference between the polarizability of the $F=3$ and the $F=4$ components of the s -states. This splitting is independent of m_F , the projection of the total angular momentum onto the quantization axis (the \hat{z} axis). From the difference in our measurements for the $F=4$ and $F=3$ lines, we determine $\alpha_{10}=0.072\pm 0.008$ MHz(kV/cm) $^{-2}$ or $290\pm 30a_0^3$. The uncertainty of this contact potential term α_{10} is dominated by the statistical uncertainty of straight-line fits of the Stark shift data.

The final terms in Eqs. (5) and (6), α_{12} and α_{02} , due to the magnetic spin-dipolar and electric quadrupole interactions, respectively, lead to a variation in the effective polarizability for the hyperfine components with different m_F . Since the population of the different hyperfine components is uniform, these terms would manifest themselves as a broadening of the Stark-shifted transition, or, if large enough, a separation of these spectral peaks from one another, but the center of gravity of the lines would remain fixed. (Redistribution of the population through optical pumping is expected to be small here because we estimate that the peak excitation rate per atom within the interaction region is only ~ 300 s $^{-1}$.) As noted in Sec. II, we do observe a broadening in our measurements of the Stark-shifted resonance, but this appears to be fully explained by the slight misalignment of the field electrodes and the resulting nonuniformity of E_0 . As an upper bound, we estimate that broadening due to α_{12} or α_{02} is $\lesssim 1$ MHz at $E_0=10$ kV/cm, yielding an upper bound on α_{12} or α_{02} of 0.02 MHz(kV/cm) $^{-2}$ or $80a_0^3$.

A calculation of the difference between the scalar polarizabilities of the $F=3$ and $F=4$ hyperfine states is much more difficult than that of the average polarizability and will be subject of a future investigation. The scalar polarizability of these states will be different only in a third-order calculation. In place of Eq. (2), this calculation includes three different third-order sums, each containing one hyperfine matrix element and two electric-dipole matrix elements. A calculation of these effects for the $6s$ state of Cs has just been published [25,26], where effects of blackbody radiation on the cesium primary frequency standard atomic clock transition were investigated. In this work, the investigators determined a difference in polarizability between the ground-state $F=4$ and $F=3$ components of $4.542\pm 0.016 \times 10^{-6}$ MHz(kV/cm) $^{-2}$. This difference is only 2.3×10^{-5} of the average ground-state polarizability. Thus, the corresponding polarizability difference for the $8s$ state becomes an interesting calculation, where our experimental results indicate a much larger relative effect.

V. CONCLUSION

In conclusion, we have reported on our joint experimental and theoretical determination of the static polarizability of the $8s^2S_{1/2}$ state of atomic cesium. The experimental ($\alpha_0=38\,060\pm 250a_0^3$) and theoretical ($\alpha_0=38\,260\pm 290a_0^3$) results are in agreement to within the 0.7% precision of each of these determinations. Our laboratory measurements for the two hyperfine components of the $8s$ -state indicate a slight ($\sim 0.8\%$) difference, yielding a polarizability difference of $\alpha_{10}=290\pm 30a_0^3$.

ACKNOWLEDGMENTS

The work of U.S. was supported in part by DOE-NNSA/NV Cooperative Agreement No. DE-FC08-01NV14050. The work of M.S.S. was supported in part by National Science Foundation Grant No. PHY-04-57078. The experimental material is based on work supported by the National Science Foundation under Grant No. PHY-0099477.

-
- [1] C. Bouchiat, C. A. Piketty, and D. Pignon, Nucl. Phys. **221**, 68 (1983).
 [2] S. L. Gilbert and C. E. Wieman, Phys. Rev. A **34**, 792 (1986).
 [3] C. S. Wood, S. C. Bennett, D. Cho, B. P. Masterson, J. L. Roberts, C. E. Tanner, and C. E. Wieman, Science **275**, 1759 (1997).
 [4] S. A. Murthy, D. Krause, Jr., Z. L. Li, and L. R. Hunter, Phys. Rev. Lett. **63**, 965 (1989).
 [5] V. Gerginov, C. E. Tanner, S. Diddams, A. Bartels, and L. Hollberg, Phys. Rev. A **70**, 042505 (2004).
 [6] E. Simon, P. Laurent, and A. Clairon, Phys. Rev. A **57**, 436 (1998).
 [7] R. J. Rafac, C. E. Tanner, A. E. Livingston, and H. G. Berry, Phys. Rev. A **60**, 3648 (1999).
 [8] S. C. Bennett, J. L. Roberts, and C. E. Wieman, Phys. Rev. A **59**, R16 (1999).
 [9] M. S. Safronova, W. R. Johnson, and A. Derevianko, Phys. Rev. A **60**, 4476 (1999).
 [10] J. M. Amini and H. Gould, Phys. Rev. Lett. **91**, 153001 (2003).
 [11] A. Derevianko and S. G. Porsev, Phys. Rev. A **65**, 053403 (2002).
 [12] V. A. Dzuba, V. V. Flambaum, and O. P. Sushkov, Phys. Lett. A **141**, 147 (1989).

- [13] S. A. Blundell, J. Sapirstein, and W. R. Johnson, *Phys. Rev. D* **45**, 1602 (1992).
- [14] A. Sieradzan, M. D. Havey, and M. S. Safronova, *Phys. Rev. A* **69**, 022502 (2004).
- [15] W. A. van Wijngaarden and J. Li, *J. Quant. Spectrosc. Radiat. Transf.* **52**, 555 (1994).
- [16] P. M. Stone, *Phys. Rev.* **127**, 1151 (1962).
- [17] J. Marek, *Phys. Lett.* **60A**, 190 (1977).
- [18] W. R. Johnson, D. Kolb, and K.-N. Huang, *At. Data Nucl. Data Tables* **28**, 333 (1983).
- [19] S. A. Blundell, W. R. Johnson, and J. Sapirstein, *Phys. Rev. A* **43**, 3407 (1991).
- [20] S. A. Blundell, W. R. Johnson, Z. W. Liu, and J. Sapirstein, *Phys. Rev. A* **40**, 2233 (1989).
- [21] A. Kreuter, C. Becher, G. P. T. Lancaster, A. B. Mundt, C. Russo, H. Häffner, C. Roos, W. Hänsel, F. Schmidt-Kaler, R. Blatt, and M. S. Safronova, *Phys. Rev. A* **71**, 032504 (2005).
- [22] M. S. Safronova and C. W. Clark, *Phys. Rev. A* **69**, 040501(R) (2004).
- [23] C. E. Moore, "Atomic Energy Levels, NSRDS-NBS 35," U.S. Government Printing Office, Washington, DC, 1971.
- [24] P. G. H. Sandars, *Proc. Phys. Soc. London* **92**, 857 (1967); and J. R. P. Angel and P. G. H. Sandars, *Proc. R. Soc. London, Ser. A* **305**, 125 (1968).
- [25] K. Beloy, U. I. Safronova, and A. Derevianko, *Phys. Rev. Lett.* **97**, 040801 (2006).
- [26] E. J. Angstmann, V. A. Dzuba, and V. V. Flambaum, *Phys. Rev. Lett.* **97**, 040802 (2006).